Planar, spherical and ellipsoidal approximations of Poisson's integral in near zone

Research Article

M. Goli*, M. Najafi-Alamdari†

Geodesy and Geomatics Engineering Dept., 1346 Valiasr Street, Mirdaamaad intersection, University of K.N.Toosi, Faculty of Civil Engineering,

Abstract:

Planar, spherical, and ellipsoidal approximations of Poisson's integral for downward continuation (DWC) of gravity anomalies are discussed in this study. The planar approximation of Poisson integral is assessed versus the spherical and ellipsoidal approximations by examining the outcomes of DWC and finally the geoidal heights. We present the analytical solution of Poisson's kernel in the point-mean discretization model that speed up computation time 500 times faster than spherical Poisson kernel while preserving a good numerical accuracy. The new formulas are very simple and stable even for regions with very low height. It is shown that the maximum differences between spherical and planar DWC as well as planar and ellipsoidal DWC are about 6 mm and 18 mm respectively in the geoidal heights for a rough mountainous area such as Iran.

Keywords:

Approximation • downward continuation • geoid • gravity anomaly • Poisson integral © Versita Warsaw and Springer-Verlag Berlin Heidelberg.

Received 3 August 2010; accepted 22 November 2010

1. Introduction

The gravimetric determination of the geoid by Stokes formula requires that the gravity anomalies to be known on the geoid and in addition, the disturbing potential being a harmonic above the geoid. To fulfill these conditions, all mass outside the geoid (topography and atmosphere) must be removed or transformed inside/on the geoid. Then, the gravity anomalies are harmonically reduced from Earth's surface downward to the geoid. This reduction is the so-called downward continuation (DWC).

In geophysical applications, the planar approximation of Poisson integral is frequently used to reduce the observed gravity on the Earth's surface to a lower level inside the Earth (Grant and West, 1965; Roy, 1966; Meyer, 1974; Fogarty, 1981; Guspí, 1987; Morgan and Blackman, 1993; Blakely, 1995; Cooper, 2004; Fedi, et al., 2005;

Hwang, et al., 2006; Xu, et al., 2007; Prutkin and Saleh, 2009).

In geodesy, the spherical Poisson integral is widely used to perform the DWC of the gravity anomalies for gravimetric geoid determination and the reduction of airborne data (Moritz, 1966; Bjerhammar, 1969, 1975, 1987; Martinec, 1996; Vaníček et al., 1996; Sun and Vaníček, 1998; Sjoberg, 2001, 2003; Huang 2002; Novak, et al., 2001; Sun, 2003; Huang et al., 2003; Huang and Veronneau, 2005). The ellipsoidal approximation of Poisson's integral was formulated and applied by Feistritzer (1997), Martinec and Grafarend (1997), Brovar et al. (2001), and Yu et al. (2003).

An unavoidable problem with DWC is the discretization of Poisson's integral. Different discretization models, point-point, mean-mean, and point-mean have been proposed by researchers: Vaníček et al., 1996, Martinec, 1996, Sun and Vaníček, 1998, Huang, 2002, 2005, Sun, 2003, Goli, et al., 2010. In the point-point model, point surface anomalies are downward continued to the point anomalies on the geoid. In the mean-mean model, mean gravity anomalies on the surface are transformed to the corresponding mean values on the geoid by a doubly averaged Poisson kernel (Vaníček et al.,

*E-mail: meh_goli@yahoo.com [†]E-mail: mnajalm@yahoo.com



1996). Finally, the point-mean model transforms the point surface anomalies to mean anomalies on the geoid.

In this study, the computation of the Poisson planar integral is compared against the spherical and ellipsoidal approximations of the integral. Since the Poisson kernel tapers off rapidly with the increasing distance from the computation point, we expect the planar approximation of the DWC could produce equivalent results to those obtained by spherical and ellipsoidal approximations. If the expectations come true, the planar approximation would be much preferred for its much shorter computation time and simple formulas.

2. Spherical and planar Poisson's integral

By the spherical Poisson's integral, a harmonic function $V[r(\Omega)]$ outside the spherical boundary (with radius R) is determined from the functional values $V(R,\Omega')$ given on the boundary (Heiskanen and Moritz, 1967) as

$$\forall \Omega \in \Omega_{0}, r(\Omega) \geqslant R : V[r(\Omega)] = \frac{1}{4\pi} \int_{\Omega_{0}} V(R, \Omega') K[r, \psi(\Omega', \Omega), R] d\Omega', \tag{1}$$

where Ω_0 is total solid angle, Ω =(θ , λ), (θ , λ) denotes the horizontal position in co-latitude and longitude, r is the radial distance. The spherical Poisson kernel $K[r(\Omega), \psi(\Omega', \Omega), R]$ is (ibid.)

$$\forall \Omega \in \Omega_{0}, r(\Omega) \geqslant R : K\left[r(\Omega), \psi(\Omega', \Omega), R\right] = R\frac{r(\Omega)^{2} - R^{2}}{d^{3}(r(\Omega), \psi(\Omega', \Omega), R)}, \quad (2)$$

where ψ and d is the angular and spatial distance between the computation point $r(\Omega)$ and the integration running point on sphere R. The point gravity anomaly multiplied by the geocentric radius at the point is a harmonic function (Heiskanen and Moritz, 1967). By applying the spherical Poisson integral for DWC of gravity anomalies, we have (Vaníček, et al., 1996):

$$\forall \Omega \in \Omega_{0}, r_{t}(\Omega) \geqslant R : \Delta g[r_{t}(\Omega)] = \frac{R}{4\pi r_{t}} \int_{\Omega_{0}} \Delta g(R, \Omega') K[r_{t}, \psi(\Omega', \Omega), R] d\Omega', \qquad (3)$$

where $r_t\left(\Omega\right)$ is the geocentric radius of the anomaly $\Delta g[r_t(\Omega)]$ on the Earth surface, and $\Delta g(R,\Omega')$ is the gravity anomalies on the geoid.

The planar approximation of Poisson integral can be derived directly using a Dirichlet boundary value problem in a Cartesian coordinate system (Grant and West, 1965; Blakely, 1995):

$$\Delta g(h) = \frac{h}{2\pi} \int_{-\infty}^{+\infty} \int_{-\infty}^{+\infty} \frac{\Delta g(x', y')}{(x'^2 + y'^2 + h^2)^{3/2}} dx' dy'. \tag{4}$$

VERSITA

where $\Delta g(h)$, $\Delta g(x',\ y')$ are gravity anomalies on the terrain and the geoid points and h is the orthometric height of the computation point. In a 3-D local Cartesian coordinate system with its origin at the sub-computation point (φ_0,λ_0) on the geoid, the relations between the spherical curvilinear and the Cartesian coordinates can be expressed as:

$$x = R(\varphi - \varphi_0),$$

$$y = R(\lambda - \lambda_0)\cos\varphi_0.$$
 (5)

The xy coordinates of computation point are (0, 0, h), see Figure 1. By changing the variables φ , λ into x, y, integral (3) becomes

$$\Delta g(h) = \frac{1}{4\pi r_t} \int_{x_1}^{x_2} \int_{y_1}^{y_2} \frac{r(\Omega)^2 - R^2}{d^3(r(\Omega), \psi(\Omega', \Omega), R)}$$

$$\Delta g(x', y') dx' dy', dx' dy' = R^2 \cos \varphi' d\varphi' d\lambda'. \tag{6}$$

Finally, the planar spherical reduced Poisson's integral reads:

$$\Delta g(h) = \frac{r(\Omega)^2 - R^2}{4\pi r_t} \int_{x_1}^{x_2} \int_{y_1}^{y_2} \frac{\Delta g(x', y')}{(x'^2 + y'^2 + h^2)^{3/2}} dx' dy'. \tag{7}$$

By assuming $r_t + R \approx 2r_t$, the integral (7) is reduced to the integral (4):

$$\Delta g(h) = \frac{(r_t - R)(r_t + R)}{4\pi r_t} \int_{x_1}^{x_2} \int_{y_1}^{y_2} \frac{\Delta g(x', y')}{(x'^2 + y'^2 + h^2)^{3/2}} dx' dy',$$

$$\approx \frac{h(2r_t)}{4\pi r_t} \int_{x_1}^{x_2} \int_{y_1}^{y_2} \frac{\Delta g(x', y')}{(x'^2 + y'^2 + h^2)^{3/2}} dx' dy',$$

$$\approx \frac{h}{2\pi} \int_{x_1}^{x_2} \int_{y_1}^{y_2} \frac{\Delta g(x', y')}{(x'^2 + y'^2 + h^2)^{3/2}} dx' dy'. (8)$$

Our numerical computations show that the differences between the integrals (7) and (4) in computing the gravity anomaly reach up to a maximum of 60 μ Gal and in terms of geoidal height differences it is up to 3 mm in a mountainous area with height h>3900 meters.

3. Ellipsoidal approximation of Poisson integral

In this section, we deal with the ellipsoidal Poisson integral in the form of ellipsoidal correction to the spherical approximation. We put into practice the methods presented by Martinec and Grafarend (1997) and by Yu, et al. (2003). The ellipsoidal coordinates

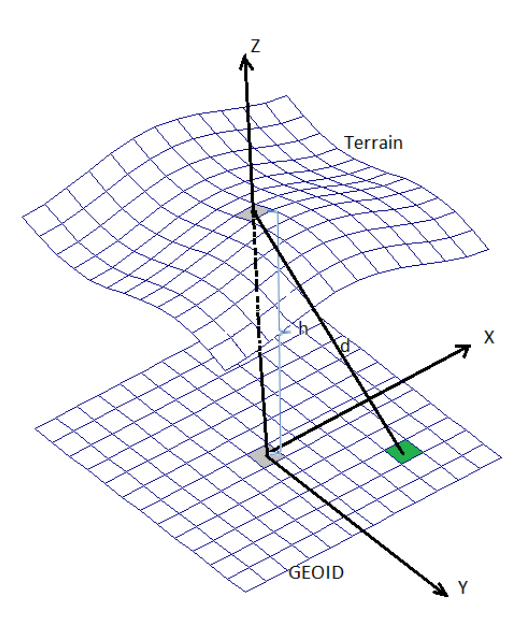


Figure 1. Local Cartesian coordinate system applied in planar DWC.

 (β, λ, u) and their relations with the Cartesian coordinates (x, y, z) (Heiskanen and Moritz, 1967) are

$$x = \sqrt{u^2 + E^2} \cos \beta \cos \lambda$$

$$y = \sqrt{u^2 + E^2} \cos \beta \sin \lambda$$

$$z = u \sin \beta,$$
(9)

where β is the reduced latitude, λ is the geocentric longitude and $E^2 = (a^2 - b^2)$ is the linear eccentricity. Analogous to the spherical case, the solution to Dirichlet boundary value problem can be written in terms of the ellipsoidal Poisson's integral (Martinec and Grafarend, 1997) as:

$$\forall \Omega \in \Omega_{0}, u \geqslant b : T(u, \Omega) = \frac{1}{4\pi} \int_{\Omega_{0}} T(\Omega') K^{ell}(\beta, \lambda, u, \beta', \lambda') d\Omega', \tag{10}$$

where b is the semi-minor axis of the ellipsoid, $d\Omega' = \cos\beta' d\lambda' d\beta'$ and $K^{ell}(\beta, \lambda, u, \beta', \lambda')$ is the ellipsoidal Poisson kernel (ibid.):

$$K^{ell} = \sum_{n=0}^{\infty} \sum_{m=-n}^{n} \frac{Q_{nm} \left(i \frac{u}{E}\right)}{Q_{inm} \left(i \frac{b}{E}\right)} Y_{nm}^*(\Omega') Y_{nm}(\Omega), \qquad (11)$$

where Q_{nm} $\left(i\frac{u}{E}\right)$ are Legendre function of the second kind, $Y_{nm}(\Omega)$ are spherical harmonics of degree n and order m (Hobson, 1955) and the asterisk denotes a complex conjugation. For practical purposes the spectral form (11) must be transformed to the closed

form. Martinec and Grafarend (1997) and Yu, et al. (2003) offered two different closed forms for K^{ell} , with an error e^4 . They have also shown that the ellipsoidal Poisson kernel can be written as the sum of the spherical Poisson kernel plus the corrections due to the ellipticity of the boundary. Also Brovar, et al. (2001) applied the effect of ellipticity on the boundary, boundary values, and on the spherical kernel. Here we implement only the two methods presented by Martinec and Grafarend (1997) and Yu, et al. (2003).

4. Discretization model

Geoid computation using the Stokes integral needs the mean gravity anomalies on the geoid. Thus, the DWC has to be implemented to transform the point anomalies measured on the Earth's surface to the corresponding mean anomalies on the geoid, $\overline{\Delta g}$ (R,Ω) . For this transformation, a single averaged kernel on the geoid, \overline{K} , is required to substitute for the original kernel in the Poisson integral. For example, in the integral (5) can be written in discrete form as (Huang, 2002):

$$\Delta g^{i} = \sum_{i=1}^{M} \overline{B_{ij}} \ \overline{\Delta g_{j}} S_{j} + \varepsilon_{D}, \tag{12}$$

where S_j is the j-th surface discretization area, ε_D is the discretization error, $\overline{\Delta g_j}$ is the mean anomaly of the geoid cell c_j and $\overline{K_{ij}}$ is average of Poisson's kernel for the geoid cell C_i computed as

$$\overline{K_{ij}} = \frac{R}{4\pi r_i} \int_{\Delta\Omega_i'} K\left[r_t, \psi\left(\Omega', \Omega\right), R\right] d\Omega'.$$
 (13)

Since there is no analytical solution for the formula above, the results of DWC depend on the numerical method employed for the evaluation of \overline{K} . One simple method is based on the midpoint quadrature method (Davis and Rabinowitz, 1984) where the domain of integration needs to be broken down to tiny small cells. However, the integral (13) can be analytically treated if the planar Poisson's kernel is assumed. Assume that (0,0,h), (x',y') are the Cartesian coordinates of terrain and geoid points in the local Cartesian system (5), see Figure 1. The integral (13) in planar approximation can be written as:

$$\overline{K_{ij}} = \frac{h_i}{2\pi} \int_{C_i} \frac{dx'dy'}{(x'^2 + y'^2 + h^2)^{3/2}}.$$
 (14)

The integral (14) can be expressed analytically as

$$\overline{K_{ij}} = \frac{1}{2\pi} \left| \arctan\left(\frac{x'y'}{h_i d}\right) \right|_{C_i}.$$
 (15)

The analytical formula for the averaged kernel facilitates the speed of computation even in the high resolution DWC.



Evaluation of Poisson's kernel at epicenter, i.e., $\psi \to 0$, is difficult as the value of the kernel increases fast. In addition, when the height of computation point approaches zero the kernel goes to infinity (Martinec, 1996; Martinec and Grafarend, 1997). Therefore the Poisson kernel, at epicenter with almost zero height, will have an extremely large value. The use of the mean Poisson kernel, K, is one practical way of solving this problem as it will be more stable than the Poisson kernel K (Sun and Vaníček, 1998; Sun, 2003, Goli, et al., 2010). It can be evaluated by breaking the cell of epicenter into very small cells. For a low altitude epicenter, the numerical value of the mean Poisson kernel is extremely sensitive to the choice of the cell breaking size. Therefore, we can use the analytical solution (15) at epicenters for solving the instability and speeding up the computations. By using Eq. (15), the mean planar Poisson kernel at epicenter becomes (Goli, et. al, 2010)

$$\overline{K_{ij}} = \frac{1}{2\pi} \arctan \left(\frac{R^2 \cos \varphi \Delta \varphi \Delta \lambda}{2h_i \sqrt{R^2 \Delta \varphi^2 + R^2 \cos \varphi^2 \Delta \lambda^2 + 4h_i^2}} \right)$$
(16

where h_i is the orthometric height of a cell on the terrain, φ is the latitude of the center of cell and $\Delta \varphi, \Delta \lambda$ denote the size of cell on the geoid along meridian and parallel, respectively.

To show the stability of solution (16) at epicenter, we compare its numerical value with those values obtained by the mean spherical Poisson kernel which is averaged at geoid cell and when is divided into sub-cells of sizes 10, 5, 1, and 0.2 arc second. Figure 2a shows these differences for the heights from 0 to 500 meters. To better focus on behavior of \bar{K} in low altitudes, the differences are plotted for the heights from 0 to 50 meters in Figure 2b. As we know, the value of \bar{K} must be decrease when increasing the height. The mean planar kernel follows this rule while the mean spherical kernel violates it for some low altitudes depending on the size of sub-cells. We do not select sub-cells with size of less 1 arc second because of computational delay. Therefore, 1 arc second can be an optimum size for the sub-cells. According to Figure 2b, since the contribution of DWC in regions with height less than 30 meters is very small we neglect doing the DWC in such areas.

5. Numerical results

A mountainous area in Iran bounded by parallels 23° $< \varphi <$ 41° and meridians 42° $< \lambda <$ 60° is selected as a test area. The very detailed global combined gravitational field model, EGM08 (Pavlis et al., 2008), up to degree/order 2160/2160 is used for generating the 5′×5′ gravity anomalies on the terrain. Figure 3 shows the topography of the test area.

The integration of the Poisson integral can be performed in two zones: near and far zones. Since the Poisson kernel decreases rapidly with the distance from a computation point, the effect of near zone can be generated sufficiently up to 1 arc degree (Huang, 2002). The effect of the far zone, amounting to several hundreds of μ Gals in extreme cases, can be reliably computed using a global

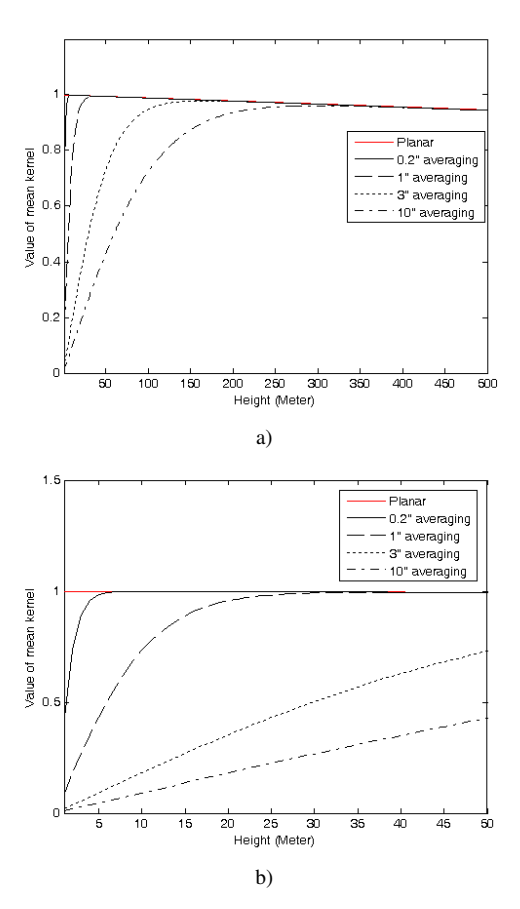


Figure 2. a) the behavior of \bar{K} when h approaches 0 for height 0 to 500, b) the behavior of \bar{K} when h approaches 0 for height 0 to 50.

geopotential model as given by Vaníček et al. (1996).

We first test the consistency of the two ellipsoidal methods given by Martinec and Grafarend (1997) and Yu, et al. (2003) to select one for further numerical tests conducted in this section. We call these method 1 and method 2 respectively. Figure 4 shows the differences of methods 1 and 2 in computing the ellipsoidal DWC of gravity anomalies. The differences never exceed 65 μ Gal in the test area, but the CPU time spent by method 1 is far less than method 2. Hence method 1 is chosen for further computations.

The correction kernel (δk) as the difference of the two ellipsoidal and spherical Poisson kernels is anisotropic. Its dependency on azimuth is very weak, and it tapers off rapidly (Ardalan, 2000, Fig. 1-1) in spherical distance so that the corresponding corrective contribution of far zones beyond $\psi>15'$ in the DWC of gravity anomalies is less than 10 μ Gal. Therefore the ellipsoidal kernel reduces to a spherical kernel beyond $\psi>15'$ and it facilitates speeding the computations.

For evaluation of differences between the three mentioned models, the DWC of gravity anomalies using planar, spherical, and

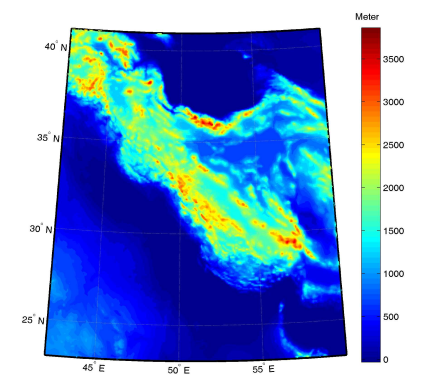


Figure 3. Topography of the test area. Unit: meter. Min = -30.090, Max = 3942.520, Mean = 757.878 and STD = 758.749

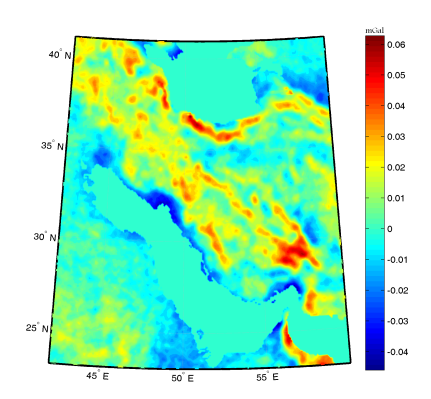


Figure 4. Differences in ellipsoidal DWC between method 1 and method 2. Unit: mGal. Min = -0.046, Max = 0.065, Mean = 0.005 and STD = 0.012

ellipsoidal (method1) are carried out in the test area. According to Figure 5a the differences between spherical and ellipsoidal DWC are correlated with topography in the area. With some exceptions (<74 μ Gal), the differences between spherical and planar solutions are minute with an RMS of 12 μ Gal, Figure 5b. According to Figures 5a and 5b the extreme values of differences take place in the regions of rough topography with low and height altitudes. This problem is due to the difficulties in computation of the mean Poisson kernel in spherical and ellipsoidal DWC in these regions. As mentioned in previous section, in these cases, the mean Poisson kernel is evaluated by breaking a geoid cell into very small cells. Different cell sizes: 10", 5", 1", and 0.2" were tested and finally 1" was selected.

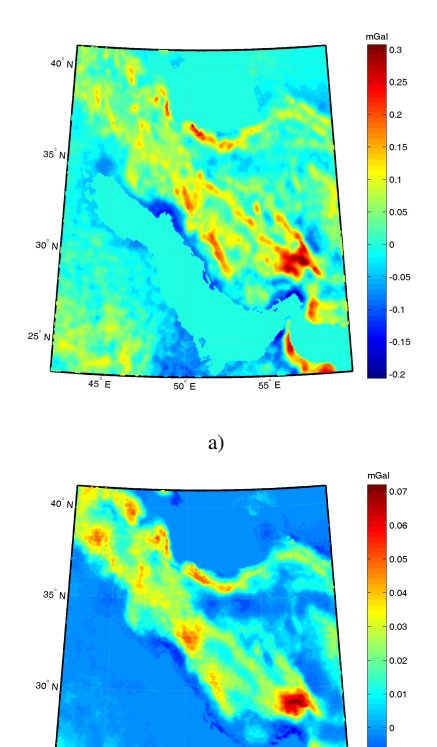


Figure 5. a) the ellipsoidal DWC minus spherical DWC. Unit: mGal. Min = -0.206, Max = 0.318, Mean = 0.021 and STD = 0.052 b) the spherical DWC minus planar DWC. Unit: mGal. Min = -0.027 , Max = 0.074 , Mean = 0.007 and STD = 0.012

b)

6. Effects on geoidal height

To show the effects of different approximations of DWC on the geoidal height, we conducted the Stokes approach for the geoid computation using the same surface gravity anomalies but different DWC models: planar, spherical, and ellipsoidal for transformation of the surface data to the geoid level. The geoid computation is divided into two parts: long-wavelength part up to the harmonic degree L=70 is achieved from the global geopotential model EGM08; the short wavelengths part (>70), i.e., the residual geoid is computed by the generalized Stokes integration (Vaniček and Cleusberg, 1987),

$$N^{70} = \frac{R}{4\pi\gamma} \iint_{\Omega_o} S^{70} (\psi) \Delta g^{70} (r_g, \Omega) d\Omega, \qquad (17)$$

extended over the spherical cap with the radius of 4° . To reduce the integral truncation error, the Molodenskij modification of Stokes kernel function, Vaníček and Kleusberg method, was adopted up



to degree L=70. Figure 6a illustrates the differences of geoids obtained as the result of spherical and ellipsoidal DWC models. Figures 6b and 6c illustrate the differences of geoids obtained as the result of planar and spherical DWC models and planar and ellipsoidal DWC models, respectively.

According to Figure 6a the spherical effect, compared to the planar, is in order of some millimeters on the geoid and can be ignored if 1 centimeter accuracy is required. Also, according to Figure 6b the effect of the differences between the ellipsoidal and the spherical DWC on the geoid does not exceed 2.5 cm at all. Therefore, all spherical and ellipsoidal solutions of DWC can be substituted by the planar solution since the planar method is much faster. Based on our developed software, the planar DWC computation time is 500 and 700 times faster than spherical and ellipsoidal computations respectively because the planar DWC uses the analytical solution of the Poisson kernel (Eq. 15) and the two other methods use the numerical integration.

Additional test can be done by comparing the geoid solutions computed by the above mentioned methods with the geoid computed by the EGM08 directly. We compared the three geoid models with EGM08 in Table 1. According to Table 1 applying the ellipsoidal DWC improves the geoid solution in some mm level against the planar and spherical DWC. There are no significant differences between the solutions using planar and spherical DWC models.

Table 1. Differences between the EGM08 geoid and the geoid models computed from different DWC solution. Unit: mm.

difference	Min	Max	Mean	STD	RMS
Planar	-45	32	5	11	13
Spherical	-49	32	7	12	14
Ellipsoidal	-43	32	3	9	10

7. Conclusions

For the computation of the geoid by Stokes's approach, the gravity anomalies must be known on the geoid surface. The gravity anomalies observed on the Earth' surface are continued downward by the Poisson's integral. The Poisson's integral is used to transform the point surface gravity anomalies to the mean anomalies on the geoid. The Poisson's integral is formulated in the local planar, spherical, and ellipsoidal coordinates in this study. We conducted an analytical solution of Poisson integration kernel for DWC in the planar coordinates for the discrete point-mean model. The result was tested against the spherical and ellipsoidal solutions both in terms of DWC values and the geoid values. There are no significant differences between the planar and spherical models of DWC in terms of both gravity anomalies and the geoid. The differences between the spherical and planar DWC, with RMS value of 12 μ Gal on 2 mm on geoid, are smaller than the differences

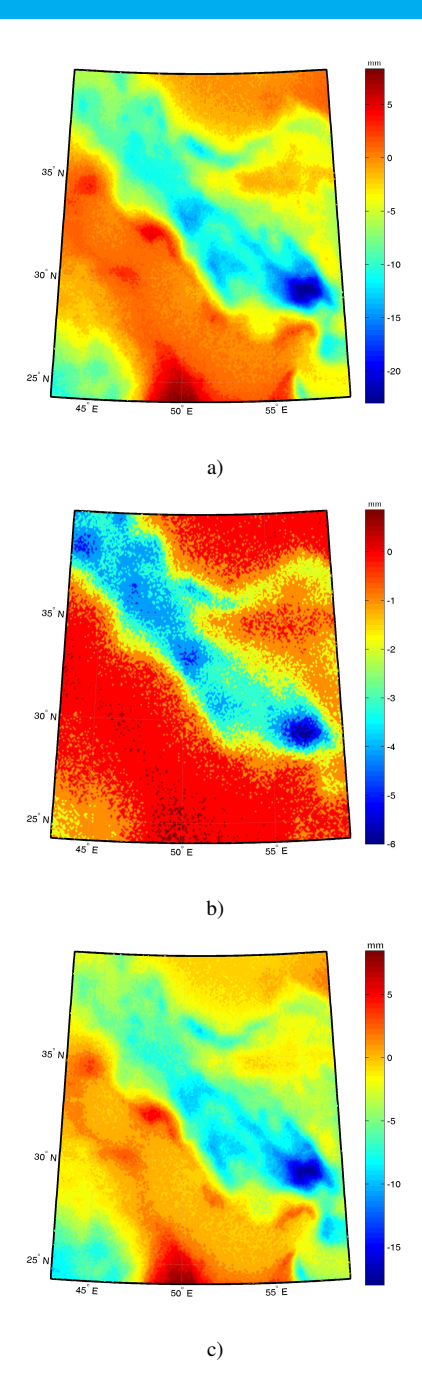


Figure 6. a) difference between spherical and ellipsoidal DWC in geoidal height. Unit: mm. Min = -23, Max = 9, Mean = 4 and RMS = 6b) difference between spherical and planar DWC in geoidal height. Unit: mm. Min = -6, Max = 1, Mean = 1 and RMS

c) difference between ellipsoidal and planar DWC in geoidal height. Unit: mm. Min = -18, Max = 9, Mean = -2 and RMS = 4



Journal of Geodetic Science

31:681-688.

between the ellipsoidal an spherical DWC. In other words, the spherical correction to planar approximation is smaller than the ellipsoidal correction to spherical approximation on both DWC of gravity anomalies and on the final geoid.

The analytical solution of Poisson kernel integration in planar approximation of DWC of gravity anomalies provides a computation of spherical and ellipsoidal Poisson's integral that is from 500 to 700 times faster. Therefore, from Table 1, neglecting the 1 cm error in the geoidal height, the spherical and ellipsoidall Poisson's integral can be replaced by the fast planar approach.

References

Ardalan A.A., 1999, High Resolution Regional Geoid Computation in the World Geodetic Datum 2000, based upon collocation of linearized observational functionals of the type GPS, gravity potential and gravity intensity, University of Stuttgart.

Bjerhammar A., 1969, On the boundary value problem of physical geodesy, Tellus, XXI, 4, 451-515.

Bjerhammar A. 1975, Discrete solutions of the boundary value problem in physical geodesy, Tellus, 2(2):97-105.

Bjerhammar A., 1987, Discrete physical geodesy, Report No. 380, Department of Geodetic Science, Ohio State University, Columbus, Ohio.

Bláha T., Hirsch M., Keller W. and M. Scheinert, 1996, Application of a spherical FFT approach in airborne gravimetry. Journal of Geodesy, 70:663-672.

Blakely R.J., 1995, Potential Theory in Gravity and Magnetic Applications, Cambridge University Press, 441.

Brovar V.V., Kopeikina Z.S., and Pavlova M.V., 2001, Solution of the Dirichlet and Stokes exterior boundary problems for the Earth's ellipsoid: Journal of Geodesy, Vol.74, 767-772.

Cheinway H., Hsiao Y. and Shih H.C., 2006, Data reduction in scalar airborne gravimetry: Theory, software and case study in Taiwan, Computers & Geosciences, 32:1573-1584.

Cooper G., 2004, The stable downward continuation of potential field data, Exploration Geophysics: 35, 260-265.

Davis P.J. and Rabinowitz P., 1984, Methods of Numerical Integration, 2nd ed. Academic Press, Orlando, FL.

Fedi M., Paoletti V., and Rapolla A., 2005, The role of multilevel data in potential field interpretation, Computers & Geosciences,

Feistritzer M., 1997, Geoidbestimmung mit geopotentiellen Koten:

Munchen Akademie der Wissenschaften.

Fogarty T., 1985, Wavenumber Filtering of Gravity Data and its Application to Interpreting Structure in the Western Transverse Ranges, California, MSc thesis, University of Southern California, Los Angeles.

Goli M., Najafi Alamdari M., and Vaníček P., 2010, Numerical behavior of downward continuation of gravity anomalies, accepted in Studia Geophysica et Geodaetica.

Guspí F., 1987, Frequency-domain reduction of potential field measurements to a horizontal plane Geoexploration, 24:87-98.

Grant F.S. and West G.F., 1965, Interpretation theory in applied geophysics, McGraw-Hill.

Heiskanen W.H., and Moritz H., 1967, Physical Geodesy: San Francisco, W.H. Freeman and Co.

Hobson E.W., 1955, The Theory of Spherical and Ellipsoidal Harmonics. New York: Chelsea.

Huang J., Sideris M.G., Vaníček P., and Tziavos I.N., 2003, Numerical investigation of downward continuation techniques for gravity anomalies: Bollettino di Geodesia e Scienze Affini, Vol. LXII, N. 1, 33-48.

Huang J., and Veronneau M., 2005, Applications of downward-continuation in gravimetric geoid modeling: case studies in Western Canada: Journal of Geodesy, Vol.79, 135-145.

Martinec Z., 1996, Stability investigations of a discrete downward continuation problem for geoid determination in the Canadian Rocky Mountains: Journal of Geodesy, Vol.70, 805-828.

Martinec Z., and Grafarend E., 1997, Construction of Green's functions to the external Dirichlet boundary-value problem for the Laplace equation on an ellipsoid of revolution: journal of geodesy, Vol.71, 562-570.

Meyer F.D., 1974, Filter Techniques in Gravity Interpretation, Original Research Article Advances in Geophysics, 17:187-261.

Morgan J.P. and Blackman D.K., 1993, Inversion of combined gravity and bathymetry data for crustal structure: A prescription for downward continuation, Earth and Planetary Science Letters, 119:167-179.



Journal of Geodetic Science

Moritz H., 1966, Linear solutions of the geodetic boundary-value problem. Report No. 79, Department of Geodetic Science, Ohio State University, Columbus, Ohio.

Novak P., Kern M., and Schwarz K.P., 2001, Numerical studies on the harmonic downward continuation of band-limited airborne gravity. Studia Geophysica et Geodaetica 45(4):327-345.

Pavlis N.K., Holmes S.A., Kenyon S.C., Factor J.K. (2008) An Earth Gravitational Model to Degree 2160: EGM 2008, presented at Session G3: "GRACE Science Applications", EGU Vienna.

Prutkin I. and Saleh A., 2009, Gravity and magnetic data inversion for 3D topography of the Moho discontinuity in the northern Red Sea area, Egypt, Journal of Geodynamics, 47:237-245.

Roy A., 1966, The method of continuation in mining geophysical interpretation Geoexploration, 4:65-83.

Sjoberg L., 2001, The effect of downward continuation of gravity anomaly to sea level in Stokes formula, Journal of Geodesy, 74:796-804.

Sjoberg L., 2003, A solution to the downward continuation effect on the geoid determined by Stokes' formula, Journal of Geodesy, 77:94-100.

Sun W., and Vaníček P., 1998, On some problems of the downward continuation of the mean Helmert gravity disturbance: Journal of Geodesy, Vol.72, 411-420.

Vaníček P. and Kleusberg A., 1987, The Canadian geoid-Stokesian approach. Manuscripta Geodaetica, Vol. 12, 86-98.

Vaníček P., Sun W., Ong P., Martinec Z., Najafi M., Vajda P., and Horst B.T., 1996, Downward continuation of Helmert's gravity anomaly: journal of geodesy, Vol. 71, 21-34.

Xu S.Z., Yang J., Yang C., Xiao P., Chen S. and Guo Z., 2007, The iteration method for downward continuation of a potential field from a horizontal plane. Geophysical Prospecting, 55:883-889.

Yu J., Jekeli C., and Zhu M., 2003, Analytical solutions of the Dirichlet and Neumann boundary-value problems with an ellipsoidal boundary: journal of geodesy, Vol.76, 653-667.

